FERROELECTRICS

Atomic-scale polarization switching in wurtzite ferroelectrics

Sebastian Calderon V[1], John Hayden[2], Steven M. Baksa[2], William Tzou[1], Susan Trolier-McKinstry[2], Ismaila Dabo[2], Jon-Paul Maria[2], Elizabeth C. Dickey[1]*

Ferroelectric wurtzites have the potential to revolutionize modern microelectronics because they are easily integrated with multiple mainstream semiconductor platforms. However, the electric fields required to reverse their polarization direction and unlock electronic and optical functions need substantial reduction for operational compatibility with complementary metal-oxide semiconductor (CMOS) electronics. To understand this process, we observed and quantified real-time polarization switching of a representative ferroelectric wurtzite ($Al_{0.94}B_{0.06}N$) at the atomic scale with scanning transmission electron microscopy. The analysis revealed a polarization reversal model in which puckered aluminum/boron nitride rings in the wurtzite basal planes gradually flatten and adopt a transient nonpolar geometry. Independent first-principles simulations reveal the details and energetics of the reversal process through an antipolar phase. This model and local mechanistic understanding are a critical initial step for property engineering efforts in this emerging material class.

Between 2019 and 2021, researchers worldwide demonstrated unexpected ferroelectricity in solid solutions in the AlN-ScN (*1*), AlN-BN (*2*), GaN-ScN (*3*), and ZnO-MgO (*4*) composition families. These reports disrupted the more than 100-year-old perspective that wurtzite crystals are pyroelectric and piezoelectric but cannot be ferroelectric because the polarization cannot be switched with an electric field. The important scientific and technological consequences that accompanied this understanding were that (i) we have a previously unknown class of ferroelectrics that violates the long-standing relationship linking polarization and ferroelectric transition temperature (*5*)—that is, they are likely not soft-mode ferroelectrics; (ii) the new physical mechanisms that enable ferroelectricity will almost certainly impart different manifestations of physical scaling trends and different property dependencies on temperature, pressure, and time; and (iii) these materials can be processed at or near room temperature with a robust property response, and in some cases (for example, $Al_{1-x}B_xN$) they consist exclusively of elements that are already common and essential in the silicon complementary metal-oxide semiconductor (CMOS) front end.

This emerging ability to directly integrate a strongly hysteretic nonlinear dielectric is transformational for future logic, memory, high-power, acoustic, or electro-optic devices (*6*–*8*). These ferroelectrics, however, bring their own challenges, the most notable being that the margin between the coercive field and breakdown field is uncomfortably small at room temperature. Consequently, devices are operated in close proximity to their failure thresholds, which invariably erodes electrical endurance and can induce degradation pathways.

Lowering the energetic switching barriers is a principal goal necessary to realize the full potential of ferroelectric wurtzites in electr optical, and acoustic devices. Empirically, we know that epitaxial tensile strain and an increased dopant concentration can reduce coercive fields in $Al_{1-x}Sc_xN$ (*9*, *10*) and $Al_{1-x}B_xN$ (*2*), presumably by reducing the energy barriers that regulate the polarity switch, and that increasing temperature also reduces the coercive field by thermally activating the nucleation and switching processes (*11*). These trends are based on macroscopic observations—that is, on measuring millimeter-scale capacitors—and although the trends demonstrate possibilities to reduce the coercive field, they do not provide local mechanistic insight.

Understanding these trends and phenomena at global and local-length scales is essential so that the property response of wurtzite ferroelectrics can be further developed for practical use. We addressed this challenge by measuring in situ the polarization reversal process at the atomic scale. Our experimental approach takes advantage of local electrostatic sample charging occurring during the illumination of dielectric materials in the electron microscope, which can induce the necessarily large local electric fields (*12*, *13*) for polarization switching in ferroelectrics (*14*, *15*). We used scanning transmission electron microscopy (STEM) in differentiated differential phase contrast mode (dDPC) to observe in situ polarization inversion in thin films of the composition $Al_{0.94}B_{0.06}N$ [(Al,B)N]. Materials in this composition space have remanent polarization (P_r) values exceeding 125 μC cm^{-2} while maintaining bandgaps above 5.8 eV; this is a substantial advantage relative to other wurtzite-based ferroelectrics, albeit the coercive fields are also larger (*2*). Our experimental analysis documents polarization switching with quantitative information at the atomic scale that is coinformed with first-principles calculations of the same composition. The first-principles simulation analyses provide an atomic-scale understanding of the switching pathways and energetics in these emerging ferroelectric materials. Covalidation

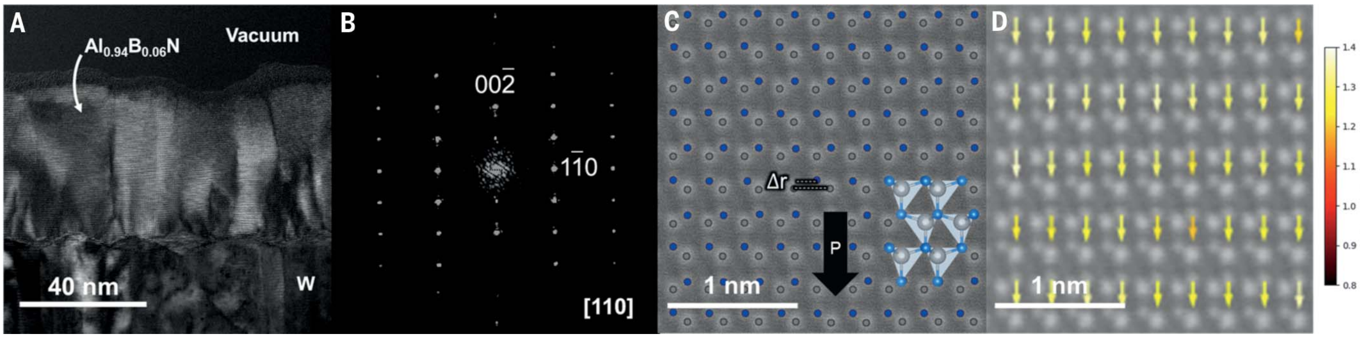

Fig. 1. Structure of (Al,B)N. (**A**) dDPC-STEM images for (Al,B)N film. (**B**) Fast Fourier transform calculated from the (Al,B)N region of image in (A). (**C**) dDPC-STEM image of an (Al,B)N grain oriented along the [110] direction, where the location of the atomic columns has been highlighted with blue (N) and gray (Al) circles after Gaussian fitting. "P" with arrow shows the direction of polarization. (**D**) dDPC image overlapped with a vector map indicating the calculated polarization at each unit cell.

---

[1] Department of Materials Science and Engineering, Carnegie Mellon University, Pittsburgh, PA 15213, USA. [2] The Pennsylvania State University, Department of Materials Science and Engineering and Materials Research Institute, University Park, PA 16802, USA.
*Corresponding author. Email: ecdickey@cmu.edu

of STEM imaging and density functional theory support a switching mechanism in which a transient antipolar structure mediates the switching process; the transient structure is similar to long-standing models for inversion domain boundaries in III-nitrides.

Effect of boron and wake-up process on the structure

We show a dDPC-STEM image of an (Al,B)N film grown by means of reactive pulsed dc sputtering on a W electrode, showing a columnar grain structure with a nominal epitaxial relation of (Al,B)N <001> // W <110> // growth direction (Fig. 1). The W electrode is faceted, and we observed small variations in the orientation of (Al,B)N grains, leading to the low density of dislocations that are observed in the image. We detected the out-of-plane crystalline mosaicity in the rocking curves of the 002 reflection of the (Al,B)N films, with full width at half-maximum (FWHM) values of 1.44° (fig. S1).

From the STEM images, we made structural polarization measurements to compare with macroscopic measurements. To quantify the spontaneous polarization, we acquired dDPC images along the <110> zone axis (Fig. 1C), where the growth direction points from the bottom to the top of the image along the $[00\bar{1}]$ direction of (Al,B)N. We determined the polarization orientation from the images by establishing the nitrogen tetrahedral orientation (Fig. 1C, inset). This orientation is polarization down—that is, the positive end of the permanent dipole points to the substrate, which is commonly referred to as an "N-polar" growth direction. Among the observed regions, the N-polar orientation is uniform with no evidence of Al-polar orientations, which is consistent with prior studies that show uniformly N-polar-oriented films (*16*). The atomic-column positions of both Al(B) and N were determined with a Gaussian fitting process on the dDPC images, which allows precise location of the atomic-column positions and thus an accurate quantification of the polarization, as previously reported (*17*). The polarization was quantified by using the Born effective charges calculated from density-functional perturbation theory (*18*). We show a vector-map representation of the calculated polarization per unit cell for an as-deposited (Al,B)N film (Fig. 1D), which we discuss in comparison with other samples.

We constructed a summary comparison of the calculated polarization per unit cell for as-deposited pure AlN film (Fig. 2A), an as-deposited (Al,B)N film (Fig. 2B), and a field-cycled (Al,B)N film left in the opposite polarity from the as-deposited film (Fig. 2C). The sputtered AlN film (Fig. 2A) exhibits an average polarization magnitude of 1.13 ± 0.07 C m^{-2}. The standard deviation is close to the measurement uncertainty arising from the atomic-column fitting process. The average measured polarization magnitude is 6.6% less than that of the ideal AlN structural model (1.21 C m^{-2}). The as-deposited (Al,B)N film (Fig. 2B) exhibits an average spontaneous polarization of 1.30 C m^{-2}, 13% larger than the undoped film, which is in agreement with the trend predicted by first principles (*2*). The (Al,B)N film exhibits peak-to-peak variations of 1.13 to 1.36 C m^{-2} and a standard deviation of 0.10 C m^{-2} within the measured area. These variations, which exceed the measurement error, are consistent with the chemical and structural inhomogeneities associated with the 6% B substitution—for example, FWHM x-ray peak widths of ~1° in ω and 2θ circles and a large radial misfit of B for Al.

Electric field–induced polarization switching from the as-deposited unipolar state can be highly frequency dependent. For kilohertz pulses just above the coercive field, full reversal per cycle may take many tens of cycles. For slow cycling (for example, 0.1 Hz), one sweep can be sufficient. This "wake-up" process that precedes fast polarization reversal is ascribed to low initial domain-wall density and mobility (*16*). To better understand this wake-up phenomenon, we completed the same STEM polarization analysis on a field-cycled sample and compared those results against bulk electrical

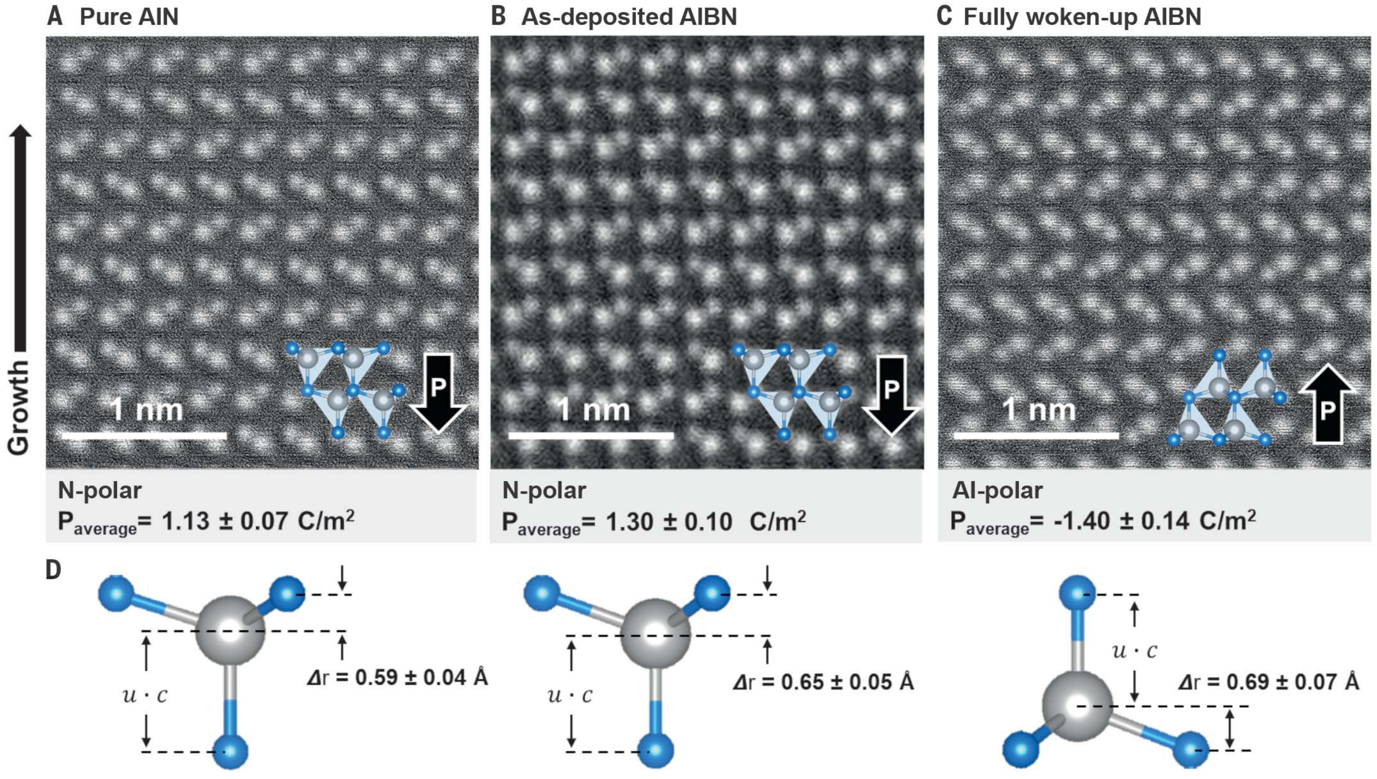

Fig. 2. Polarization evolution. (**A** to **C**) dDPC images for (A) pure AlN, (B) (Al,B)N as-deposited, and (C) field-cycled (Al,B)N. (**D**) Schematic of the structure modification after boron incorporation and field cycling. dDPC-STEM images showing the full field of view are presented in fig. S2.

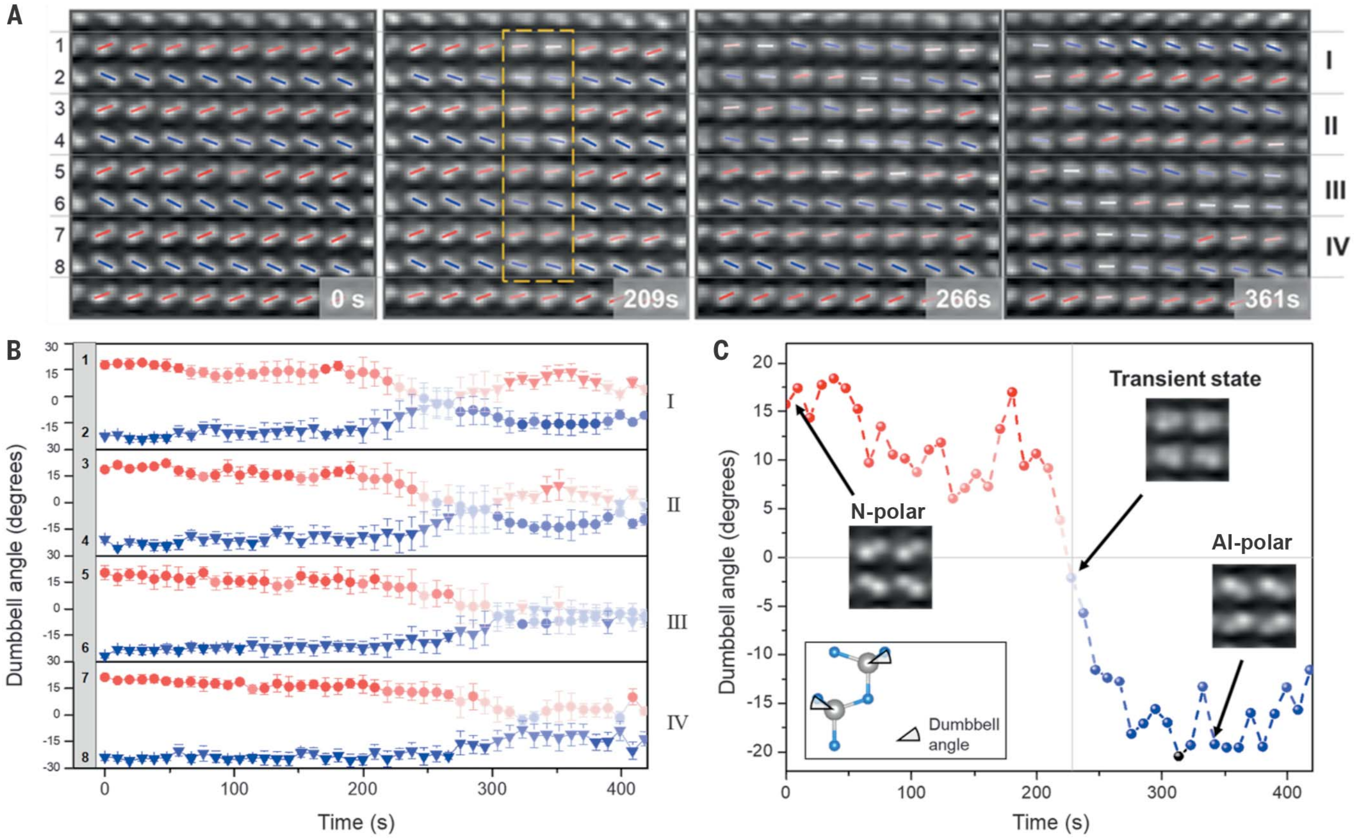

Fig. 3. In situ polarization switching. (**A**) dDPC-STEM frames at 0, 209, 266, and 361 s for in situ polarization switching. (**B**) AlN dumbbell-angle evolution as a function of time for the corresponding frames in (A). The Roman numerals in (A) and (B) indicate the different regions in the images going from the top of the frame (I) to the bottom (IV). The rows of AlN dumbbells in the images are numbered from 1 to 8 for reference between (A) and (B). (**C**) Dumbbell-angle evolution as a function of time for one unit cell. (Inset) The schematics of the dumbbell angle and the dDPC images at specific times.

measurements. For a fully woken-up sample, hysteresis loops yield P_r of 1.38 ± 0.01 C m^{-2}, whereas dDPC-STEM imaging yields 1.40 ± 0.14 C m^{-2}. Furthermore, the STEM-based polarization measurements allow us to compare the intrinsic spontaneous polarization in the as-deposited and field-cycled states (Fig. 2, B and C). The similarity of these STEM-quantified polarization magnitudes (average values within ~7%) suggests that the wake-up process does not substantially alter the bulk material structure.

To further explore this possibility, we analyzed the average local structure evolution using two-dimensional vector pair correlation functions (vPCF) calculated from dDPC-STEM images that can be found in the supplementary materials (fig. S3) (*19*). The relevant parameter extracted from vPCF is Δr (Fig. 2D), which describes the distance between the nearest (Al,B) basal-plane layers and N layers, also referred to as the "puckering" of the wurtzite basal planes. Whereas the average Δr increases 10% on alloying AlN with 6% B, the Δr in as-deposited and field-cycled (Al,B)N states are the same within one standard deviation of the measurement distribution, supporting the conclusion of no major structural phase transitions during the wake-up process. We therefore infer that the wake-up phenomenon is more likely associated with interfacial or nucleation site–based mechanisms than bulk crystal-structure changes.

In situ switching observations

Electron microscopy can visualize ferroelectric polarization reversal at length scales that reveal local atomic and domain structures (*15*, *20*). In these cases, preparation of extremely thin parallel-plate capacitor structures that can be field cycled either in situ or by implementing a nanoprobe that applies a local bias is common (*20*). Wurtzite ferroelectrics are difficult to analyze with these methods because of the large coercive fields that invariably accelerate surface migration of atomic species across the sample surface and create short-circuit pathways. Alternatively, prior reports demonstrate that the charge accumulation from beam-solid interactions in electron and ion microscopes can create internal fields large enough to reverse ferroelectric polarization (*14*, *15*). By using extended beam exposures during STEM image acquisition, polarization reorientation can be achieved from the large lateral electric fields that emerge from the beam-solid interactions that produce positive sample charging, as described in detail by Cazaux (*12*). For very thin samples, incident electrons do not contribute substantially to charge accumulation because they are fully transmitted. However, some electrons are scattered inelastically, promoting ionization and secondary and Auger electron emission and a net positive charge accumulation for electrically insulating materials. This superimposes additional built-in electric fields, which can reach the megavolt-per-centimeter range needed to switch (Al,B)N. Our primary dataset is an in situ domain switching movie collected on an (Al,B)N film (movie S1). We summarize the in situ data with a set of frames spanning the roughly 7-min experiment (Fig. 3). The images are indexed from top to bottom with row numbers and divided into four regions (I, II, III, and IV), with region I closest to vacuum (the top of the sample), where the charge-induced field is expected to be largest in the vertical direction (and thus capable of inducing switching), and region IV closest to the bottom electrode, which provides a physical path to

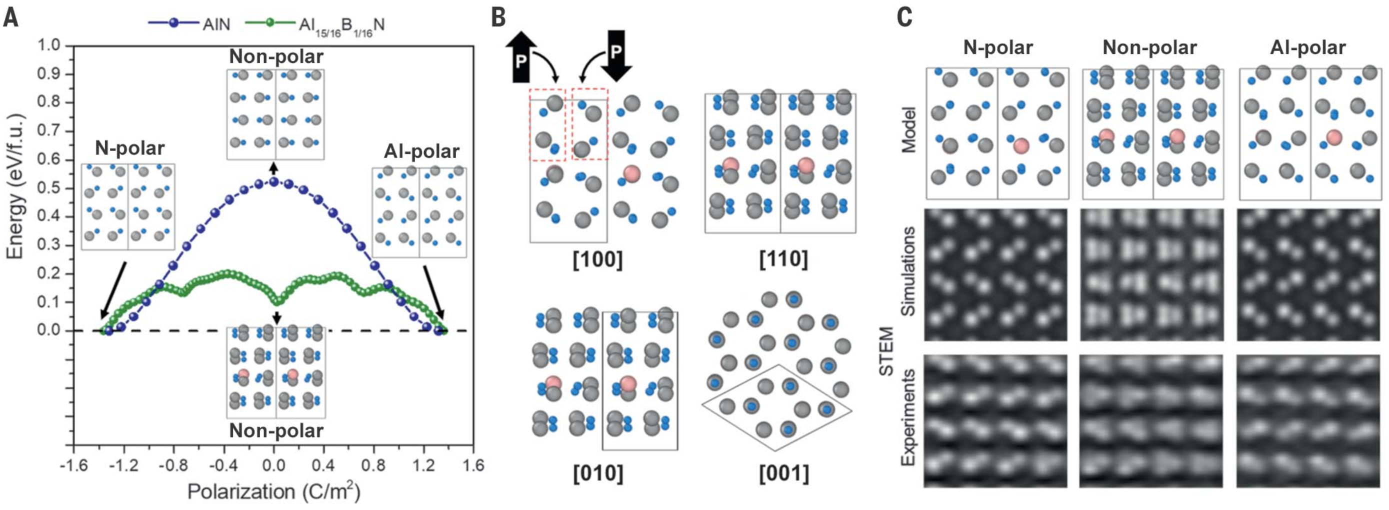

Fig. 4. Nudged-elastic-band simulation of polarization reversal pathways. (**A**) Nudged-elastic-band simulation of polarization reversal pathways for AlN and $Al_{15/16}B_{1/16}N$. (Insets) The structural models at specific stages of the simulation. (**B**) Structural model of the nonpolar transient state calculated for $Al_{15/16}B_{1/16}N$ viewed along different projections. (**C**) Atomic models, STEM image simulations, and experimental images for the N-polar, nonpolar, and Al-polar states.

microscope ground. This distinction is important because the electric field in the experiment will necessarily be spatially heterogeneous in magnitude and evolve over time; nonetheless, it serves as an important mechanism to induce switching in these large-coercive-field samples. Our STEM images are overlayed with red, white, and blue lines, which indicate quantitatively (from image analysis) the dumbbell angles associated with the bond puckering in the wurtzite basal plane; red is positive, blue is negative, and white is 0° on average. We show four graphs that quantify the average dumbbell angles for regions I through IV (Fig. 3B), each one representing a unit-cell-thick layer. We note four observations: (i) In region I, the transition between red and blue is the most clear and uniform and occurs first; this observation is consistent with expectations for maximum charging fields in this zone. (ii) As one progresses from the top zones to the bottom zones, the dumbbell-angle transition is less uniform, and the switching process takes longer; this is again consistent with the anticipated electric-field evolution and gradient direction. (iii) Region IV and below do not completely switch, which is attributed to diminishing electric field toward the bottom of the sample. (iv) The regions of the sample that switch do so through a transient state in which the integrated intensities of all associated scatterers yield an average dumbbell angle of 0° (Fig. 3C).

We also note the 209-s panel in Figure 3A, and in particular, the yellow highlighted rectangular region where the largest electric field is expected. The dumbbell-angle rotation, and thus switching, initiates first at the top of this rectangle and progresses laterally and vertically with time; the structure in this region is identified as a local domain nucleation site with attendant domain walls.

Last, we show the average AlN dumbbell-angle progression for one unit cell in the movie close to the location of maximum anticipated electric field (Fig. 3C). The angle evolution from positive to negative values, and thus polarization down to up, is clearly visible. Figure 3C also contains inset images of the initial N-polar (polarization-down) state, the final Al-polar (polarization-up) state, and the transient intermediate state of this region of the sample.

To further understand the switching pathway and identify the transient state observed experimentally, we carried out first-principles calculations using the nudged-elastic-band method for determining the minimum energy pathway for polarization reversal in both AlN and $Al_{15/16}B_{1/16}N$, which closely matches the experimental composition. After structural optimization, we calculated the polarization reversal pathways (Fig. 4A). The results highlight two distinct mechanisms, in which AlN switches coherently in one step at 0.523 eV/formula unit (f.u.), whereas $Al_{15/16}B_{1/16}N$ switches sequentially in nine steps at 0.200 eV/f.u. The coherent polarization reversal suggests that pure AlN switches through a nonpolar hexagonal (*h*)-BN–like structure, whereas in $Al_{15/16}B_{1/16}N$, we observed an average nonpolar supercell in the middle of the switching process (Fig. 4A, insets). This metastable state is not a *h*-BN–like structure but consists of antipolar arrangements of wurtzite motifs when viewed along the [100] direction, as shown in our atomic models (Fig. 4B). A more convoluted structure is observed when projecting the structure along the [110] or [010] orientation (Fig. 4B), where N-polar and Al-polar unit cells are overlapped in this projection, which agrees qualitatively well with the transient structure observed during the in situ switching experiments. Both in situ data and first-principles calculation independently show that the anion and cation sublattice contribute comparable distortions along the switching path.

To correlate the experimental observations and the first-principles calculations, we carried out dPDC-STEM image simulations using the atomic models of the $Al_{15/16}B_{1/16}N$, at the initial (N-polar), middle (nonpolar), and final (Al-polar) step in the simulation (Fig. 4C). The simulated images correlate well with the experimental STEM images at different stages during the switching process, corroborating the nonpolar state predicted with the nudged-elastic-band simulations. Similar projected local structures have been observed with TEM and STEM images in polarity inversion domain boundaries (IDBs) in other wurtzite structures (*21*–*23*), and the four- and eightfold rings of bonds that were found in simulations of IDBs in GaN (*24*) are present in this metastable $Al_{15/16}B_{1/16}N$ structure (fig. S4). The low-energy IDB in GaN exhibits no interface electronic gap states because the Ga and N atoms can maintain similar local coordination as the parent wurtzite phase.

These results provide insight into the induced ferroelectricity of wurtzite structures such as AlN, where the incorporation of alloying elements, such as B, in the parent wurtzite structure, results in substantial local-bonding and local-structural distortions, as has been pointed out in the (Al,Sc)N system (*25*). We demonstrated that this disorder provides low-energy pathways to nucleate the switching process and that the switching is mediated by a metastable transient nonpolar state. This nonpolar metastable state maintains a local structure similar to the parent wurtzite structure and analogous to the local structure evidenced in IDBs in numerous nonferroelectric wurtzites. The chemical and structural disorder in the (Al,B)N alloys leads to a relatively flat energy landscape that facilitates switching.

Our work provides detailed atomic-scale structure analysis of ferroelectrically active wurtzite-structured (Al,B)N thin films, revealing that B doping leads to a larger spontaneous polarization relative to pure AlN sputtered films. The study also unambiguously shows the domain nucleation and switching pathway for these emerging ferroelectric materials. The alloying disorder provides a complex but substantially lower-energy-barrier switching pathway to a transient nonpolar state, which engenders ferroelectricity in the class of technologically important polar materials. Such wurtzite-structured materials can be coprocessed with mainstream semiconductors, providing pathways toward CMOS-compatible integrated ferroelectrics, piezoelectrics, and electro-optics. Our insights into the atomic-scale processes of domain switching provide guidance to ongoing and future investigations of wurtzite-structured thin films that can lead to targeted property performance.

REFERENCES AND NOTES

1. S. Fichtner, N. Wolff, F. Lofink, L. Kienle, B. Wagner, *J. Appl. Phys.* **125**, 114103 (2019).
2. J. Hayden *et al*., *Phys. Rev. Mater.* **5**, 044412 (2021).
3. D. Wang, P. Wang, B. Wang, Z. Mi, *Appl. Phys. Lett.* **119**, 111902 (2021).
4. K. Ferri *et al*., *J. Appl. Phys.* **130**, 044101 (2021).
5. S. C. Abrahams, S. K. Kurtz, P. B. Jamieson, *Phys. Rev.* **172**, 551–553 (1968).
6. A. Sebastian, M. Le Gallo, R. Khaddam-Aljameh, E. Eleftheriou, *Nat. Nanotechnol.* **15**, 529–544 (2020).
7. N. Setter *et al*., *J. Appl. Phys.* **100**, 051606 (2006).
8. A. Fernandez *et al*., *Adv. Mater.* **34**, e2108841 (2022).
9. M. Noor-A-Alam, O. Z Olszewski, M. Nolan, *ACS Appl. Mater. Interfaces* **11**, 20482–20490 (2019).
10. S. Clima *et al*., *Appl. Phys. Lett.* **119**, 172905 (2021).
11. W. Zhu *et al*., *Appl. Phys. Lett.* **119**, 062901 (2021).
12. J. Cazaux, *Ultramicroscopy* **60**, 411–425 (1995).
13. R. F. Egerton, P. Li, M. Malac, *Micron* **35**, 399–409 (2004).
14. A. C. G. Nutt, V. Gopalan, M. C. Gupta, *Appl. Phys. Lett.* **60**, 2828–2830 (1992).
15. J. L. Hart *et al*., *Phys. Rev. B* **94**, 174104 (2016).
16. W. Zhu *et al*., *Adv. Electron. Mater.* **8**, 2100931 (2022).
17. S. Calderon, S. D. Funni, E. C. Dickey, *Microsc. Microanal.* **28**, 1–12 (2022).
18. Materials and methods are available as supplementary materials.
19. S. D. Funni *et al*., *APL Mater.* **9**, 091110 (2021).
20. L. Li, L. Xie, X. Pan, *Rep. Prog. Phys.* **82**, 126502 (2019).
21. T. Akiyma *et al*., *Jpn. J. Appl. Phys.* **58** (SC), SCCB30 (2019).
22. N. Stolyarchuk *et al*., *Sci. Rep.* **8**, 14111 (2018).
23. L. T. Romano, J. E. Northrup, M. A. O'Keefe, *Appl. Phys. Lett.* **69**, 2394–2396 (1996).
24. J. E. Northrup, J. Neugebauer, L. T. Romano, *Phys. Rev. Lett.* **77**, 103–106 (1996).
25. K. Yazawa, J. S. Mangum, P. Gorai, G. L. Brennecka, A. Zakutayev, *J. Mater. Chem. C* **10**, 17557–17566 (2022).
26. S. Calderon *et al*., Atomic-scale polarization switching in wurtzite ferroelectrics - dDPC data, Zenodo (2023); https://doi.org/10.5281/zenodo.7916420.
27. S. Calderon *et al*., Atomic-scale polarization switching in wurtzite ferroelectrics - DFT data, Zenodo (2023); https://doi.org/10.5281/zenodo.7916565.

ACKNOWLEDGMENTS

Funding: This material is based on work supported by the Center for 3D Ferroelectric Microelectronics (3DFeM), an Energy Frontier Research Center funded by the US Department of Energy, Office of Science, Office of Basic Energy Sciences Energy Frontier Research Centers program under award DE-SC0021118. E.C.D. and S.C. acknowledge the use of the Materials Characterization Facility at Carnegie Mellon University supported by grant MCF-677785. **Author contributions:** Conceptualization: S.C.V. and E.C.D. Material production: J.H. and J.-P.M. Electron microscope characterization: S.C.V, W.T., and E.C.D. First-principles calculations: S.M.B. and I.D. Data interpretation: S.C.V., J.H., S.M.B., E.C.D., J.-P.M., I.D., and S.T.-M. Funding acquisition: E.C.D, J.-P.M., I.D., and S.T.-M. Supervision: E.C.D., J.-P.M., and I.D. Writing – original draft: S.C.V. Writing – review and editing: All authors reviewed and edited the draft. **Competing interests:** The authors declare that they have no competing interests. **Data and materials availability:** TEM data generated in this study are available at Zenodo (*26*). First-principles data and models that support the findings of this study are available at Zenodo (*27*).

SUPPLEMENTARY MATERIALS

science.org/doi/10.1126/science.adh7670
Materials and Methods
Figs. S1 to S4
Movie S1
References (*28–44*)

Submitted 13 March 2023; accepted 10 May 2023
10.1126/science.adh7670

Atomic-scale polarization switching in wurtzite ferroelectrics

Sebastian Calderon, V, John Hayden, Steven M. Baksa, William Tzou, Susan Trolier-McKinstry, Ismaila Dabo, Jon-Paul Maria, and Elizabeth C. Dickey

Science **380** (6649), . DOI: 10.1126/science.adh7670

Editor's summary
Nitride-based ferroelectric wurtzites are an emerging family of crystals that are highly attractive as switching materials for modern microelectronics. The chemistry of these materials is a good match for current semiconductor platforms. Calderon *et al*. used an array of characterization tools to determine exactly how a representative wurtzite composed of aluminum, boron, and nitrogen undergoes polarization switching. A more detailed understanding of this process is vital for lowering the electric field under which these materials switch, because this is a limiting factor in moving them into applications. —Brent Grocholski

Science (ISSN 1095-9203) is published by the American Association for the Advancement of Science. 1200 New York Avenue NW, Washington, DC 20005. The title *Science* is a registered trademark of AAAS.